IEEE Access
Multidisciplinary ⋮ Rapid Review ⋮ Open Access Journal

Received May 21, 2021, accepted May 27, 2021, date of publication June 3, 2021, date of current version June 15, 2021.

Digital Object Identifier 10.1109/ACCESS.2021.3085989

The Magnetic Energy Harvester With Improved Power Density Using Saturable Magnetizing Inductance Model for Maintenance Applications Near High Voltage Power Line

BUMJIN PARK[1], SUNGRYUL HUH[1], JONGWOOK KIM[1], HAERIM KIM[1], YUJUN SHIN[1], SEONGHO WOO[1], JAEHYOUNG PARK[2], ANDRES BRITO[1], DONGWOOK KIM[3], (Member, IEEE), HYUN HO PARK[4], (Senior Member, IEEE), OKHYUN JEONG[5], (Member, IEEE), JA-IL KOO[6], AND SEUNGYOUNG AHN[1], (Senior Member, IEEE)

[1]The Cho Chun Shik Graduate School of Green Transportation, Korea Advanced Institute of Science and Technology, Daejeon 34051, South Korea
[2]Hardware Engineering Group, Samsung Electronics, Suwon 16677, South Korea
[3]Department of Automotive Engineering, College of Mechanical and IT Engineering, Yeungnam University, Gyeongsan 38541, South Korea
[4]Department of Electronic Engineering, The University of Suwon, Hwaseong 18123, South Korea
[5]Department of Electronic Engineering, Sogang University, Seoul 04107, South Korea
[6]Ferraris Inc., Las Vegas, NV 89119, USA

Corresponding author: Seungyoung Ahn (sahn@kaist.ac.kr)

This work was supported in part by the Ministry of Science and ICT (MSIT), South Korea, through the Information Technology Research Center (ITRC) Support Program supervised by the Institute for Information & Communications Technology Planning & Evaluation (IITP) under Grant IITP-2021-2016-0-00291, and in part by the Korea Electric Power Corporation under Grant R20XO02-35.

ABSTRACT Recently, maintenance applications around power lines have been actively studied. These applications usually supply power through magnetic energy harvesting(MEH) to devices around the power line. A major challenge for practical MEH is to overcome magnetic saturation, which can cause degradation of power density under a wide current range in the power line. In this paper, we propose a design methodology to harvest maximized output power by considering the saturation effect. To consider magnetic saturation, the output power model and the saturable magnetizing inductance model based on magnetizing current were comprehensively analyzed. Additionally, the critical point of saturation for the maximum harvested power was analyzed by considering different primary side current conditions. With the proposed design methodology, the accuracy and efficiency of the output model were verified with experimental results compared to the conventional model. To consider the real environment, a 150 kW class of AC resistor load bank was implemented to control the primary current from 0 to 100 A with power frequency of 60 Hz. Experimental results show that the proposed method can harvest an average power of 14.32 W on 70 A power line, which is an increase of 39.8 % compared with the conventional design method.

INDEX TERMS Energy harvesting, magnetic material, magnetic saturation, smart sensor, power supply, power line, smart grid.

I. INTRODUCTION

Power systems are one of the greatest engineering achievements and the largest industrial assets in human history. Worldwide, power systems are experiencing a period of sustained growth to meet growing energy consumption. Especially, the expansion of the electric vehicle market and the economic expansion of countries have led to an increase in the demand for electrical energy. The increasing demand for electric power requires larger and more complex power systems. As power systems becomes larger and more complex, the importance of inspection and maintenance to improve the reliability of power systems is rapidly increasing [1].

Generally, power lines span millions of kilometers in length and cross vast expanses of natural environments. Utility assets may incur damage from natural hazards such

The associate editor coordinating the review of this manuscript and approving it for publication was Ahmed Aboushady.

as fallen trees, wildfire, and so on. To maintain reliability and high efficiency of a wide range of utility assets, constant inspection and preventive maintenance are required near power lines. However, most inspection and maintenance work is still done manually. Since power lines are often mounted in hostile environments, the work is extremely dangerous and insecure for the technical personnel. Moreover, another big concern is that almost 45%-65% of senior utility engineers are at or close to retirement, and there will soon be a manpower shortage due to a lack of young talent entering the field [2]. Therefore, transmission system operators are motivated to implement monitoring and maintenance systems that reduce human interference [2], [3]. To overcome these problems, there are various types of devices around power lines such as smart sensors [4]–[6], climbing robots [7]–[9], visual cameras [10], [11] and wireless charging stations for drone [12], [13], as shown in Fig. 1. These devices enable engineers to maintain high reliability and to oversee a wide range of power grids through maintenance applications. They can also reduce maintenance costs and eliminate human exposure to dangerous environments. However, although these devices can improve work efficiency, they require an independent power source to ensure continuous operation. Most of them rely heavily on battery power, which has a finite capacity and high cost and suffers the inconvenience of changing the battery periodically which, in the process, increases maintenance cost. To solve these limitations, energy harvesting technology is an alternative solution to make systems self-sustainable [14], [15].

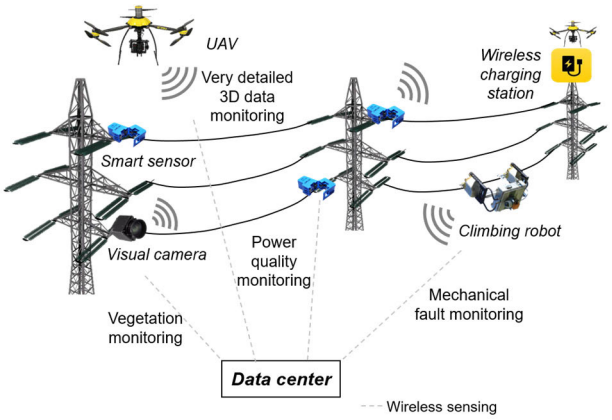

FIGURE 1. Various type of devices applied to power lines for constant inspection and preventive maintenance tasks.

There are various energy source candidates for use in devices near power lines, such as solar, wind, electromagnetic fields, and so on. Photovoltaic devices are easily installed and have high power density during direct sunlight. However, these devices are strongly affected by weather conditions. Moreover, they require periodic maintenance, such as to eliminate dust and dirt on the solar panels. Wind energy harvesting systems using small wind turbines can convert kinetic energy into electric energy. However, similar to photo-voltaic devices, output performance is affected by weather conditions. Vibration generation devices using the piezoelectric effect are not affected by weather condition, but have extremely low power density, as well as durability problems [16]. In recent years, magnetic energy harvesting(MEH) using electromagnetic induction has been actively researched [17]–[23]. This system produces electric energy through the alternating magnetic field around the power line. Compared to other energy harvesting methods, the output power is independent of weather conditions and easy to install without any maintenance; it also has a relatively high power density. Taken together, it is concluded that magnetic energy harvesters are the most suitable method for stable power supply near power lines.

However, from a practical point of view, MEH has a problem with magnetic saturation, which is related to power density. The main feature of MEH is that the current flow-in in the power line fluctuates over a wide range of tens to thousands of amperes. It is challenging to harvest power over a wide current range with high power density and stable output because the magnetic core can become saturated. When the magnetic core is saturated, magnetic flux does not change, and harvesting power drops to zero. To prevent saturation over a wide range, a large air gap is used, but this causes the power density to decrease.

At the same time, the output of equipment to aid maintenance near the power lines is also increasing. Especially, industrial robots and drone charging stations [24] require large output, beyond a few milliwatts. Even though magnetic field energy harvesting has better power density than other methods, it still has low power density. In the case of a climbing robot with a 40 W power rating, a harvester of 40 kg or more is required [25]. However, the size and weight of the online device are strictly regulated by utility safety standards [26] because their weight can cause mechanical effects such as additional un-desired sag, and so on. Therefore, the only way to solve the above problems is to improve the power density of MEH under a wide current range.

These challenges have not yet been addressed. Indeed, the majority of existing work has focused on maximizing the harvested power for fixed current conditions and narrow current range. In [27], the researchers concluded that induced voltage is the most important factor in design because DC power at the output is dependent on this voltage. To obtain maximized induced voltage, mu-metal, of which the permeability is over 200,000, was used. However, mu-metal is too expensive to commercialize and is not suitable for clamp structures due to its brittle characteristics. Moreover, it is not practical for MEH be-cause the primary current condition is fixed and saturation is not considered. In [28], to avoid saturation effects under a wide current range, large air gap and dissipative resistor are employed. This method prevents saturation and enables harvesting in a wide current range. However, it has low power density at average current because the air gap is determined based on the maximum primary current. It is difficult to apply when the difference between the maximum

and average current is large. Additionally, the output model assumes a no-load condition, and so it is not accurate if the load condition changes. In [23], a novel method to improve power density is proposed using an artificial magnetic field produced by an additional power management circuit. This system generates a counter magnetic field to prevent saturation; the magnetic core is not driven into the saturation region, and more energy can be harvested. However, the implementation of the additional circuit will make the system bulky and complex. Moreover, the main limitation of this work is that it is assumed that primary current and magnetizing inductance are fixed.

In this paper, we propose a practical design methodology for MEH with improved power density by considering load conditions in a wide current range. For the first time, we control the load voltage to maximize the power harvested from the power lines by considering the saturation effect. To consider the saturation effect in the output model, the effect of magnetizing inductance variation was analyzed through a saturable inductance model based on the B-H curve.

Consequently, our research differs from and extends conventional works in many respects:

1. Improved power density over a wide range of power line currents

2. Accurate output model through saturable magnetizing inductance model

The paper is organized as follows: Details on the output power model obtained by considering magnetic saturation are given in Section II. In Section III, the experiment and results of the proposed design are presented. In Section IV, the discussion is presented. Finally, the conclusion is given in Section V.

II. ANALYSIS OF LOAD VOLTAGE TO MAXIMIZE OUTPUT POWER IN MEH

The fundamental concept of MEH is illustrated in Fig. 2. According to Faraday's law, a time-variant current is capable of generating an alternating magnetic field. Then, the generated magnetic field induces AC voltage at the coil terminals.

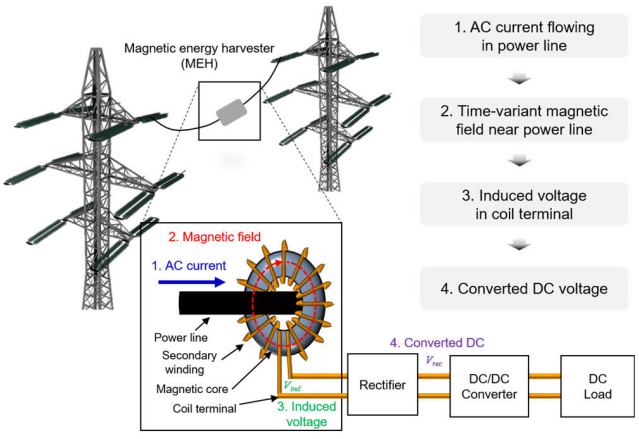

FIGURE 2. Fundamental concept and structure of MEH installed on power line.

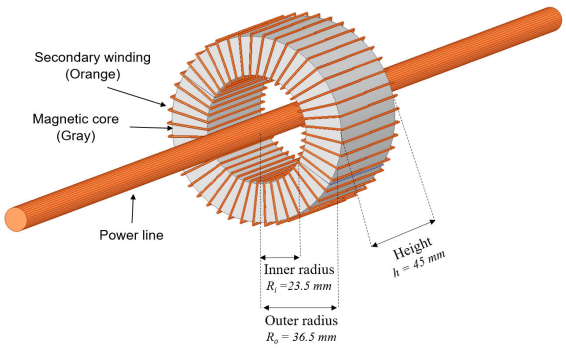

FIGURE 3. Magnetic energy harvester structure and dimensions of magnetic core.

In this process, the output voltage is converted to DC voltage through the rectifier and DC/DC converter. Finally, the converted DC voltage is supplied to applications. Fig. 3 shows the structure and dimensions of the magnetic core. A soft magnetic material is used for the core material, such as ferrite, electrical steel, or an amorphous material.

This section is organized as follows. In Section A, the output model of the MEH under unsaturated condition is analyzed using a constant magnetizing inductance. In Section B, to consider the saturated condition, a model of saturable magnetizing inductance is proposed based on the real model of the *B-H* curve. Finally, in Section C, the output model obtained by considering the saturated condition is analyzed using the proposed model of saturable magnetizing inductance.

A. OUTPUT MODEL WITH CONSTANT MAGNETIZING INDUCTANCE

The circuit model of the MEH was developed using the practical transformer model [29] shown in Fig. 4(a). For simplicity of circuit analysis, a magnetizing inductance L_m is used instead of mutual inductance. The parasitic components such as leakage inductance and core loss component can be negligible if the permeability of the magnetic material is extremely large [17].

In this case, the ripple is ignored and the primary side voltage V_{pri} is determined as secondary side voltage V_{sec} divided by secondary turns N_s. All circuit components are reflected on the primary side and then analyzed as shown in Fig. 4(b).

The average harvested output power P_o can be determined as follows:

$$P_o = \frac{1}{0.5T_p}\int_{t_s}^{t_s+0.5T_p} V_{rec}\frac{(i_{pri}(t)-i_{L_m}(t))}{N_s}dt = \frac{1}{0.5T_p}\int_{t_s}^{t_s+0.5T_p}\frac{V_{rec}i_{har}(t)}{N_s}dt \quad (1)$$

where T_p is the period of the primary side and t_s is the start time of the harvesting current. V_{rec} is the rectifier voltage across the DC/DC converter.

The waveforms of i_{pri} and i_{Lm} represent the primary current and magnetizing current, respectively, as shown in Fig. 5(a).

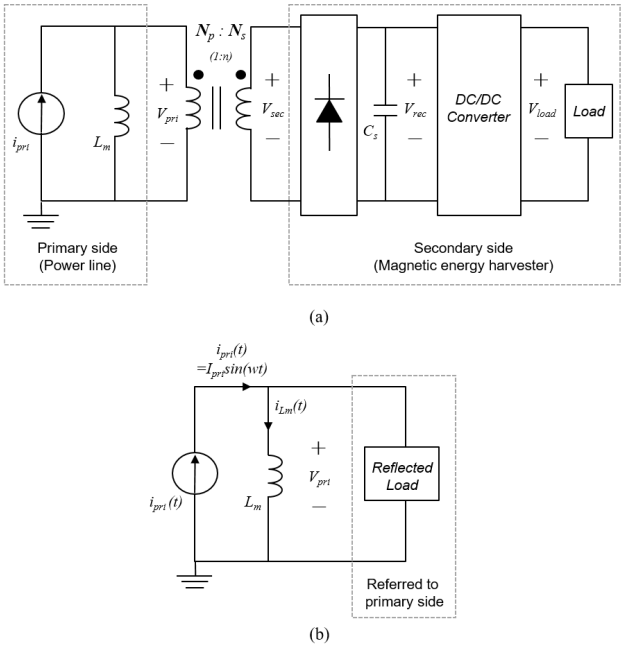

FIGURE 4. Simplified equivalent circuit of MEH. (a) Equivalent circuit of proposed MEH. (b) Approximated equivalent circuit reflected to primary side.

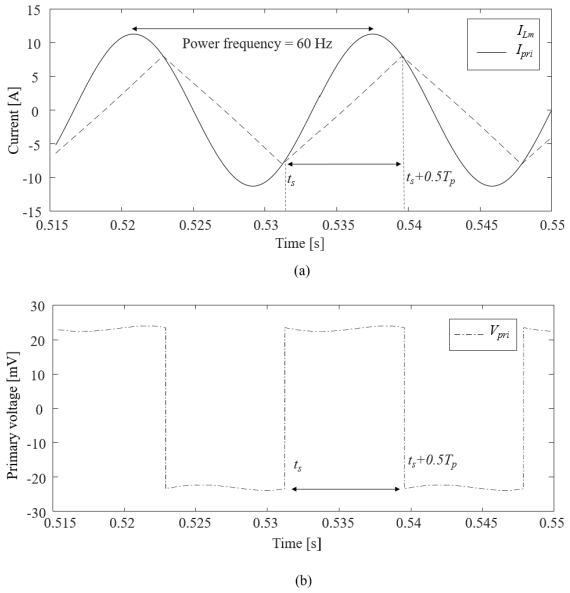

FIGURE 5. Time-domain waveform relationship between primary side current, magnetizing current, and primary voltage. (a) Waveforms of I_{Lm} and I_{pri}. (b) Nearly constant primary voltage during half cycle.

The harvested power current i_{har} is the difference between i_{pri} and i_{Lm}. Fig. 5(b) shows the waveform of V_{pri} considering active components using circuit simulation(PSIM).

First, to ensure volt-second balance for the inductor, the ripple of i_{Lm} can be derived as follows:

$$\Delta i_{L_m} = \frac{\int_{t_s}^{t_s+0.5T_p} V_{pri} dt}{L_m} \cong \frac{V_{pri} \cdot 0.5T_p}{L_m} \tag{2}$$

Assuming that the load is connecting the super-capacitor C_s through a rectifier and DC/DC converter, the load voltage V_{load} can be considered as a constant DC voltage.

To determine t_s, we can use the relationship between i_{pri} and i_{Lm}. Since i_{pri} is equal to i_{Lm} at t_s, the peak value of the magnetizing current i_{Lm}^{pk} can be expressed as follows:

$$i_{pri}(t_s) = i_{L_m}(t_s) \tag{3}$$

$$I_{pri} \sin(\omega_o t_s) = i_{L_m}(t_s) = -i_{L_m}^{pk} \tag{4}$$

where w_o is the primary side angular frequency and I_{pri} is the peak value of the primary side current.

Since the offset of i_{Lm} is zero, the magnetic energy stored in the magnetic core over $0.5T_p$ is zero. So, i_{Lm}^{pk} can be established as half of the ripple of i_{Lm}:

$$i_{L_m}^{pk} = 0.5 \cdot \Delta i_{L_m} = \frac{V_{pri} \cdot T_p}{4L_m} \tag{5}$$

(4) can be rewritten by substituting (5) for i_{Lm}^{pk} as follows:

$$i_{L_m}^{pk} = I_{pri} \sin(\omega_o t_s) = -\frac{V_{pri} \cdot T_p}{4L_m} \tag{6}$$

In summary, the start point of harvesting time t_s can be found as follows:

$$t_s = -\frac{1}{\omega_o} \sin^{-1}\left(\frac{V_{pri} \cdot T_p}{4L_m I_{pri}}\right) \tag{7}$$

The start time of harvesting depends on not only the magnetizing inductance L_m and the primary side current I_{pri}, but also on the primary side voltage V_{pri}.

The output power of the load is calculated by substituting (7) for t_s. (1) can be rewritten as follows:

$$\begin{aligned} P_o &= \frac{2V_{rec}I_{pri}}{T_p N_s} \int_{t_s}^{t_s+0.5T_p} \sin(\omega_o t) dt \\ &= \frac{4\sqrt{2}V_{rec}i_{pri,rms}}{T_p N_s \omega_o} \cos(\omega_o t_s) \\ &= \frac{2\sqrt{2}V_{pri}i_{pri,rms}}{\pi} \cos(\omega_o t_s) \end{aligned} \tag{8}$$

where $i_{pri,rms}$ is the root-mean-square(rms) value of the primary side current. The secondary side voltage V_{sec} is equal to the rectified voltage V_{rec} in conduction mode.

In conventional work, L_m has been assumed to be extremely large and the arcsine term for t_s converges to zero. For this reason, high permeability materials were inevitably used to increase power density of the MEH.

Thus, (8) can be expressed as follows:

$$P_o = \frac{2\sqrt{2}}{\pi} V_{pri} i_{pri,rms} \tag{9}$$

Making an assumption that magnetic core parameters and primary current are fixed in the unsaturated region, P_o is determined by V_{pri}.

The maximum P_o can be found at $V_{pri,max}$ by taking the derivative of (8) with respect to V_{pri}.

$$\left.\frac{\partial P_o}{\partial V_{pri}}\right|_{V_{pri,\max}} = 0 \Rightarrow V_{pri,\max} = \frac{4L_m i_{pri,rms}}{T_p} \tag{10}$$

where $V_{pri,max}$ is the primary voltage at which maximum P_o can be harvested.

Thus, the maximum harvested output $P_{o,max}$ can be rewritten as follows:

$$P_{o,\max} = \frac{8L_m}{\pi T_p} i_{pri,rms}^2 \tag{11}$$

According to (11), the maximum harvested power increases with primary side current and magnetizing inductance.

However, magnetic saturation should be considered according to the primary side current. When the magnetic core is operated in saturated condition, magnetizing inductance changes dramatically. Equations (8)-(11) do not take into account the saturated condition, so they are only valid in the linear condition. Therefore, V_{pri} must be operated under saturation voltage. The saturation voltage V_{sat} can be derived as follows:

$$V_{sat} = 4A_{eff} B_{\max} f N_p \tag{12}$$

where B_{max} is the saturation flux density and A_{eff} is the cross-sectional area of the magnetic core. The detailed derivation of the equation is provided in Appendix A.

Moreover, using the relationship between (10) and (12), the saturation boundary condition for i_{pri} is calculated as follows:

$$i_{sat,pri} = \frac{B_{\max} l_{eff}}{\mu_0 \mu_r N_p} \tag{13}$$

where μ_o is the permeability of free-space and μ_r is the relative permeability of the magnetic core; B_{max} is the maximum magnetic flux density, which depends on the characteristics of the core material. The length of the magnetic field path and the number of primary winding turns are defined as l_{eff}, and N_p, respectively.

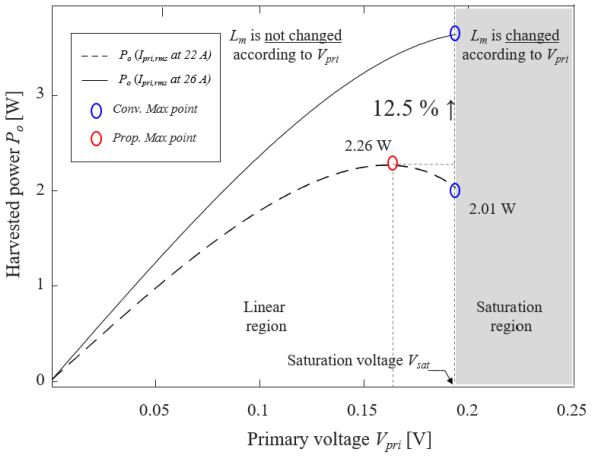

FIGURE 6. Harvested power P_o response with primary voltage V_{pri}, based by Equations (8) to (11). As the primary side current increases, the primary voltage that generates the P_o increases.

Consequently, when $i_{pri,rms}$ is smaller than $i_{sat,pri}$, $V_{pri,max}$ can be derived from Equation (10). Fig. 6 provides an example with different primary side current conditions and $i_{sat,pri} = 26.5$ A. For each primary current magnitude, under condition of unsaturated operation and constant L_m, there exists only one optimal load voltage. In case of 22 A, optimal load voltage for the maximum harvested power is 2.26 W at 0.16 V.

As the primary side current increases, the point of maximum harvested power approaches the saturation point. This means that $V_{pri,max}$ changes according to the primary side current. However, when $i_{pri,rms}$ exceeds $i_{sat,pri}$, Equations (8)-(11) are not valid due to the changes of magnetizing inductance values in the saturation region. In this case, V_{sat} is the operating voltage needed to generate maximum harvested output. Compared with that of the conventional method, the power density is improved by 12.5%. The output model of the MEH is summarized in TABLE 1.

TABLE 1. Output model according to primary side current.

Case	Output model
$i_{pri,rms} < i_{sat,pri}$	(11)
$i_{pri,rms} > i_{sat,pri}$	(8) @ V_{sat}

B. MODELING OF SATURABLE MAGNETIZING INDUCTANCE BY CONSIDERING MAGNETIC SATURATION AND LOAD CONDITION

In the linear operation region of the B-H curve, L_m can be expressed as follows:

$$L_m = \frac{\mu_0 \mu_r A_{eff}}{l_{eff}} N_p^2 \tag{14}$$

If the relative permeability has a constant value, L_m is determined only using the magnetic core dimensions and number of coil windings according to (14).

When the primary side current is sufficient to saturate the magnetic core, the relative permeability of the magnetic core no longer has a constant value. The magnetic core is operated in the saturation region, where, because there are no changes in magnetic flux, the relative permeability decreases sharply and converges to a low value. In other words, a magnetizing inductance model that can consider changes in relative permeability according to primary side current is required. So, (8) to (11) are valid only when the magnetic core operates in a linear region of the B-H curve.

Through the B-H curve shown in Fig. 7(a), which expresses the characteristics of the magnetic properties, the magnetizing inductance can be represented as a function of the current in fixed conditions. Since the magnetic flux density B is proportional to the flux linkage λ, and the magnetic field intensity H is proportional to the magnetizing current, the B-H curve can represent the relationship between flux linkage λ and magnetizing current i_{Lm} instead, as shown in Fig. 7(b). The inductance is defined as the ratio of the flux linked with the coil to the current flowing through it. In the $\lambda - i_{Lm}$ curve, the gradient is the magnetizing inductance

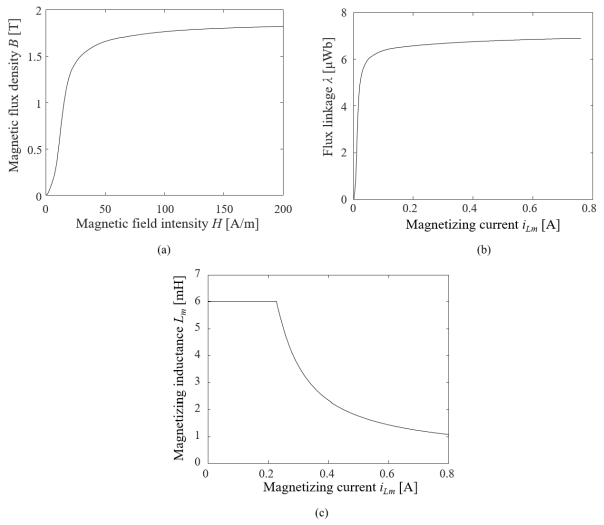

FIGURE 7. Relationship between B-H curve, flux linkage versus magnetizing current, and magnetizing inductance versus magnetizing current. (a) B-H curve, (b) $\lambda - i_{Lm}$ curve, (c) $L_m - i_{Lm}$ curve.

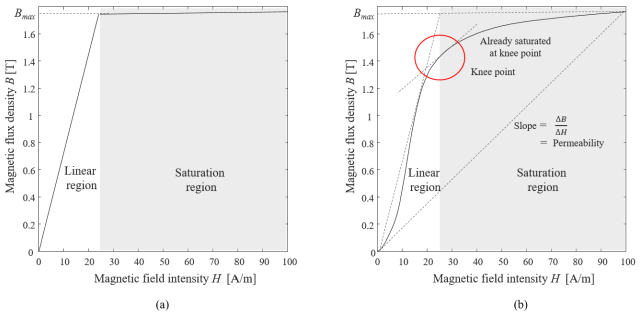

FIGURE 8. B-H curves in linear region and saturation region. (a) Piecewise linear model, (b) real model.

according to the magnetizing current. As a result, the $\lambda - I_{Lm}$ curve can be substituted for the $L_m - i_{Lm}$ curve, as shown in Fig. 7(c).

Under saturated operation, the value of magnetizing inductance is governed by not only the structural characteristics of the magnetic core but also the magnetizing current in saturated operation. Chung *et al.* proposed a general inductance model in [30] that provides a mathematical expression to include the saturation phenomenon. This model is based on the piecewise *B-H* curve, which is divided into saturation and linear regions. In this case, the relative permeability remains constant until B_{max} is reached, as shown in Fig. 8(a).

However, it is not practical to define saturation at the point where B_{max} is reached. In the practical magnetic material, the magnetic saturation has already started at the knee-point of the *B-H* curve, as shown in Fig. 8(b). The knee-point magnetic flux density B_{knee} is not the same as B_{max}. Especially, in the section between the magnetic flux density at the entrance of the knee point and the maximum magnetic flux density, the changes in permeability according to magnetizing current cannot be accurately considered. Moreover, according to [17], maximum output power can be harvested when the core is in the vicinity of the saturation point, the so-called 'Soft Saturation Region(SSR)'. If the model in [30] is used, it is not possible to accurately track the point at which maximum harvested power is generated. If the SSR is not accurately predicted, the MEH is operated beyond the SSR, resulting in a dramatically reduced power density. Therefore, it is necessary to accurately model the magnetizing inductance as a function of the magnetizing current i_{Lm} based on the measured results of the *B-H* curve.

The conventional model [30] of saturable inductance based on the piecewise linear model of the *B-H* curve can be expressed as:

$$L_{m,sat(con)} = \frac{2L_m}{\pi}\left(\sin^{-1}\left(\frac{I_{sat}}{I_{pri}}\right) + \frac{I_{sat}}{I_{pri}}\sqrt{1-\left(\frac{I_{sat}}{I_{pri}}\right)^2}\right) \quad (15)$$

The detailed derivation of the equation is provided in Appendix B. However, although this model can simply represent the saturation effect under no-load conditions, it cannot accurately consider changes in magnetizing current i_{Lm} according to load conditions. Therefore, the saturable inductance should be modeled by considering the changes of magnetizing inductance according to i_{Lm} and V_{pri}.

The proposed model of saturable magnetizing inductance $L_{m,sat}$, based on measurement results, can be expressed as:

$$L_{m,sat} = \frac{2L_m}{\pi}\left(\sin^{-1}\left(\frac{i_{sat}(V_{pri,knee})}{i_{L_m}}\right) + \frac{i_{sat}(V_{pri,knee})}{i_{L_m}}\sqrt{1-\left(\frac{i_{sat}(V_{pri,knee})}{i_{L_m}}\right)^2}\right) \quad (16)$$

With the inductor's saturation current $i_{sat}(V_{pri,knee})$ expressed as,

$$i_{sat,Lm} = \left|\frac{V_{pri,knee}}{Z_{L_m}(V_{pri,knee})}\right| \quad (17)$$

where $V_{pri,knee}$ is the primary voltage at the knee point. $i_{sat}(V_{pri,knee})$ is the saturation magnetizing current when $V_{pri,knee}$ is applied to L_m. Z_{Lm} is the impedance of L_m, which depends on V_{pri} according to the primary side current. $2L_m/\pi$ is used to normalize the function to the constant L_m when the magnetic core is in the working linear region.

As shown in Fig. 9, the point $V_{pri,knee}$ is defined as the V_{pri} at which a 10% increase in applied voltage increases i_{Lm} by 50% based on IEC 61869-2(Instrument transformer-part2) [34]. When the applied voltage condition is $V_{pri,knee} > V_{pri}$, $L_{m,sat}$ has constant value L_m. Other than that, $L_{m,sat}$ is governed by the ratio of $i_{sat}(V_{pri,knee})$ to i_{Lm}. $L_{m,sat}$ sharply decreases when V_{pri} exceeds $V_{pri,knee}$. i_{sat} and $V_{pri,knee}$ are determined based on measurements involving an open-circuit test using a power meter. The change in the magnetizing inductance value, which depends on V_{pri}, can be estimated by Equations (16)-(17). It is noteworthy that i_{Lm} increases considerably even for small increments in applied voltage across the magnetizing inductance. Therefore, for maximum

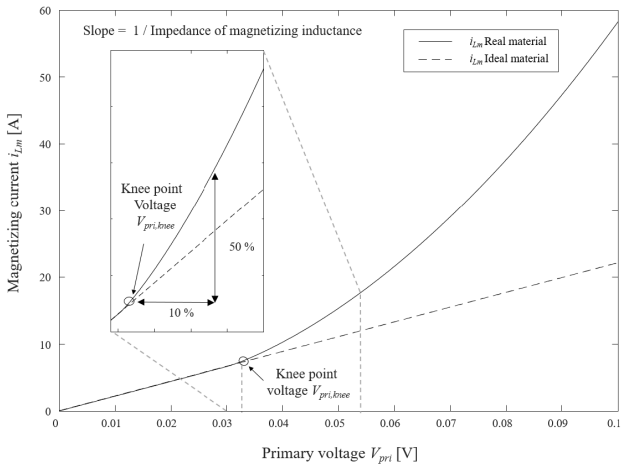

FIGURE 9. Magnetizing current i_{Lm} response with primary voltage V_{pri}. Knee point voltage of MEH is expressed by referring to IEC 61869-2. As primary voltage increases, when knee point voltage is exceeded, magnetizing current increases rapidly.

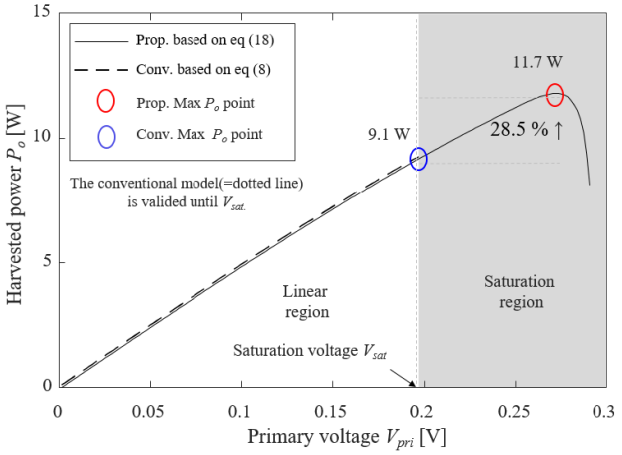

FIGURE 10. Harvested power P_o response with primary voltage V_{pri} based on Equation (19). Conventional model based on constant magnetizing inductance has a maximum harvested power point at V_{sat}. In proposed model, maximum harvested power is generated in saturation region.

harvested power, V_{pri} should be selected by considering the effect on magnetic saturation.

C. OUTPUT MODEL WITH SATURABLE MAGNETIZING INDUCTANCE

To consider the saturation region, the output model can be rewritten by substituting saturable magnetizing inductance $L_{m,sat}$ for constant magnetizing inductance L_m. Therefore, (7) can be rewritten by substituting (16) for L_m, as follows:

$$t_{eff} = -\frac{1}{\omega_o}\sin^{-1}\left(\frac{V_{pri}T_p}{4L_{m,sat}I_{pri}}\right) \tag{18}$$

To consider the saturated condition, the effective harvested power $P_{o,eff}$ can be rewritten by substituting (18) for (7), as follows:

$$P_{o,eff} = \frac{2\sqrt{2}V_{pri}i_{pri,rms}}{\pi}\cos(\omega_o t_{eff}) \tag{19}$$

For a given I_{pri}, the parameter P_o is also dependent on the values $L_{m,sat}$ and t_{eff}. The numerical calculation of the response of P_o to V_{pri} was compared with those of the conventional model [28], [29] and of measurements. Fig. 10 provides an example at $i_{pri,rms} = 55$ A, $N_s = 60$, $i_{sat,pri} = 26.5$ A, $i_{sat,Lm} = 0.353$ A, and power frequency $= 60$ Hz, respectively. The core parameters are as follows: Outer radius of core $= 36.5$ mm, Inner radius of core $= 23.5$ mm, height of core $= 45$ mm.

In this case, since $i_{pri,rms}$ is larger than $i_{sat,pri}$, $V_{pri,max}$ cannot be derived from Equation (10). In the conventional method, the maximum harvested power can be obtained at V_{sat}, as mentioned above in Section II. Both models have a similar tendency in that the harvested power is proportional to V_{pri} until the magnetic core is saturated. However, in the proposed method based on the saturable magnetizing inductance model, the output can be predicted beyond the saturation region.

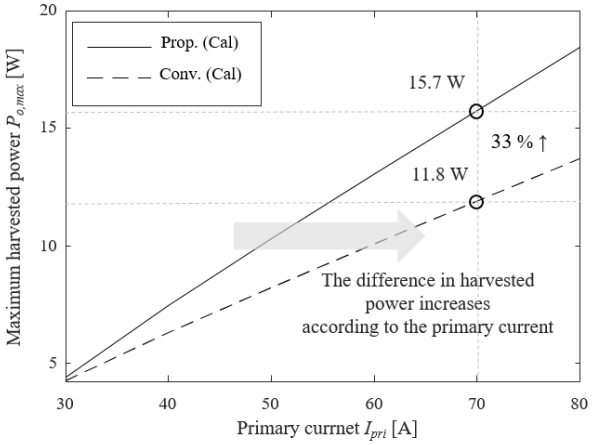

FIGURE 11. Maximum harvested power $P_{o,max}$ response with primary side current I_{pri}. In proposed model, as primary current increases, difference in harvested power increases compared with conventional method [27]–[29].

As a result, the maximum harvested power can be obtained at the SSR. The maximum harvested power is 11.7 W at 0.267 V, which is an improvement of 28.5 % compared with the conventional method. More importantly, as V_{pri} increases over the SSR, the harvested power decreases because the reactive power increases. Therefore, in consideration of the magnetic saturation, it is necessary to design the MEH based on the magnetizing current and load voltage.

Moreover, the maximum harvested power of the MEH is analyzed according to different primary currents. Fig. 11 shows the relation between maximum harvested power shown in Fig. 10 and primary current. As the primary current increases, the difference in harvested power between the proposed method and the conventional method increases. For example, when the primary current is 70 A, the difference in harvested power is 3.9 W. This means that the power density improves by 33 % compared with the conventional method.

By using the proposed model, no large air gap or additional windings are required to prevent magnetic core saturation. In addition, the proposed method can reduce the volume of the magnetic core. This makes it possible to improve the power density more simply than with the conventional model. The output model of the MEH considering the magnetic saturation is summarized in TABLE 2.

TABLE 2. Output model considering magnetic saturation.

Case	Output model
Conventional model	(8) @ V_{sat}
Proposed model	(19)

III. EXPERIMENTAL VERIFICATION AND RESULTS

To verify the proposed design methodology, an experimental platform was built as shown in Fig. 12. In this process, it was important to emulate a controllable source of the magnetic field. The experimental platform is built by considering the EPRI (Electric Power Research Institute) technical report [33] and related paper [20].

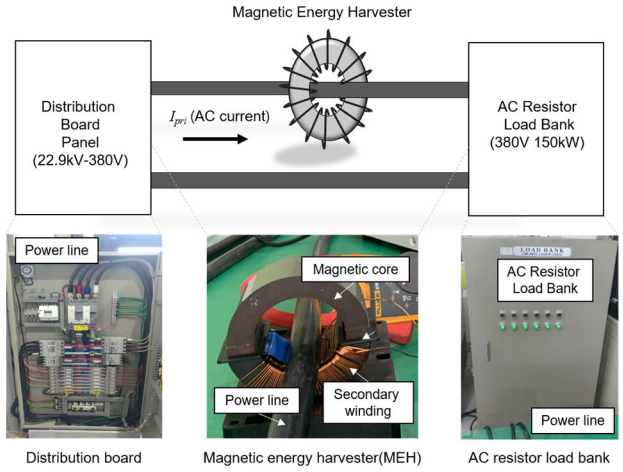

FIGURE 12. Experimental platform for controllable source of magnetic field. This was based on an EPRI technical report, which is related to test bed development for power harvesting.

To emulate a real environment, a 380V 3-phase distribution panel was directly connected to the AC resistor load bank. The 150 kW level of the AC resistor load bank makes it possible to control the primary current from 0 to 100 A with power frequency of 60 Hz. The primary side current is sourced through a short-circuit conductor loop external to the unit and is controlled by a personal computer. It was supplied through a single wire to consider the window space in the MEH. This method is more practical than those in conventional research [19], [27], which used a source with ampere-turns and a lot of windings. The Cold-rolled electrical steel was used as the core material and μ_r and B_{max} were estimated from the measured B-H curve. The dimensional parameters of the magnetic core are listed in TABLE 3.

TABLE 3. Dimensional parameters of magnetic core.

Symbol	Parameter	Value
R_o	Outer radius	36.5 mm
R_i	Inner radius	23.5 mm
h	Height	45 mm
R_{mid}	Middle radius	30 mm
A_{eff}	Cross-sectional area of core	540 mm^2
L_{eff}	Magnetic flux path length	185 mm
N_s	Secondary winding	60
L_m	Magnetizing inductance (Primary)	29.1 uH ~ 33.3 uH
	Magnetizing inductance (Secondary)	105 mH ~ 120 mH
f	Power frequency	60 Hz
μ_r	Relative permeability (Linear)	8,355
B_{max}	Maximum magnetic flux density	1.5 T

A. EXPERIMENTAL RESULTS FOR MAXIMUM HARVESTED POWER IN UNSATURATED CONDITION

The prototype was implemented to verify that the proposed method achieved maximum harvested power in unsaturated condition. The measurement setup is as shown in Fig. 13. The magnetic core is clamped to the power line. As explained in the previous section, to emulate a power line environment, the current of the power line is sourced through the distribution panel and the AC resistor load bank. The secondary coil is connected to the full-bridge rectifier, which converts AC voltage into DC voltage. The capacitor is placed parallel to the electronic load to smooth the load voltage. To control the load voltage, electronic load(KIKUSUI PLZ1004W) was used.

To confirm the waveform, an oscilloscope (Keysight MSO-X 4154A) was used to conduct the output measurement test. Fig. 14 shows the experimentally measured P_o and the calculated P_o at the adjusted V_{pri} when primary current is 22 A. In unsaturated condition, it is obvious that the calculated harvested power and experimental results have the same tendency. This means that the load voltage of the MEH for maximum harvested power can be accurately predicted according to the theoretical analysis presented in Section II.

In the conventional design method [30], the output power is 1.9 W in the vicinity of the saturation voltage. By applying the proposed design method, output of 2.18 W, which is an increase of 14.7 % of the output power is achieved. We also confirmed that $V_{pri,max}$ occurs before the saturation voltage V_{sat}. From this comparison, the proposed design method can be seen to have an advantage of improved power density without using any additional core material.

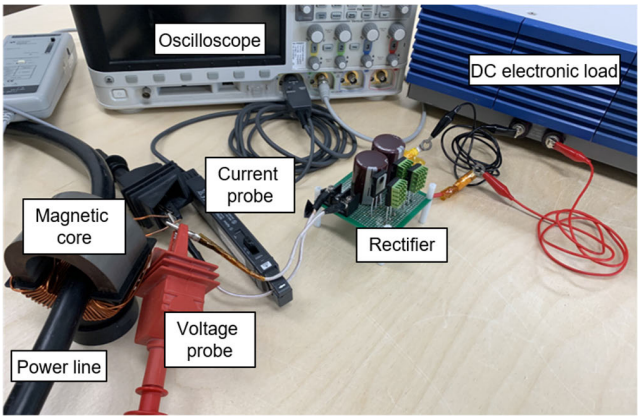

FIGURE 13. Measurement setup of variation of harvested power P_o according to primary side current and primary voltage.

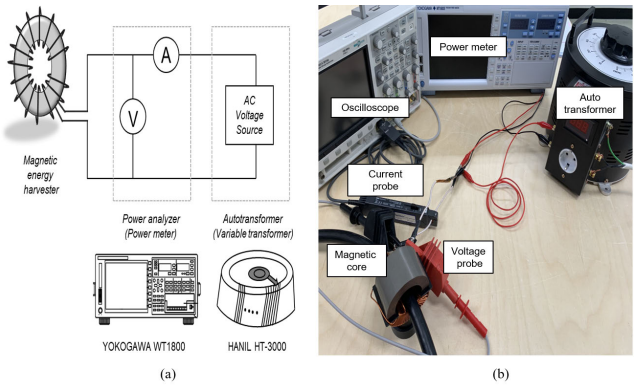

FIGURE 15. Measurement setups to extract Norton circuit parameter (magnetizing inductance). (a) diagram of open-circuit test, (b) measurement setup.

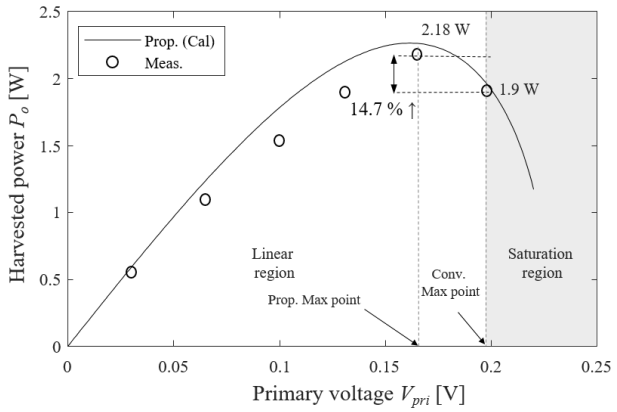

FIGURE 14. Numerical calculations and measurement results of harvested power P_o according to primary voltage V_{pri} in unsaturated conditions.

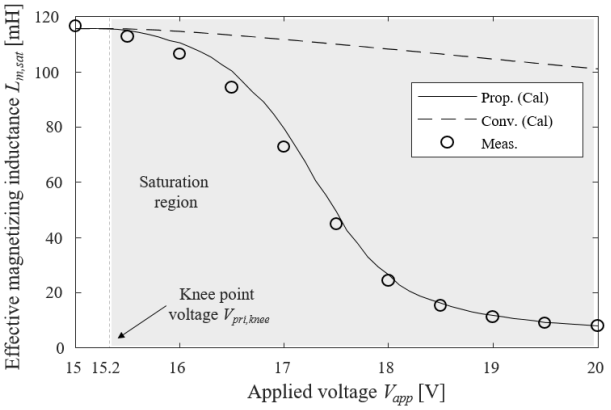

FIGURE 16. Measurement results of saturable magnetizing inductance $L_{m,sat}$ according to applied voltage V_{app}.

B. MODEL OF SATURABLE MAGNETIZING INDUCTANCE BY CONSIDEING SATURATION CONDITION

To verify the proposed model for saturable magnetizing inductance, described in Section II, an experiment was conducted. The saturation condition in the magnetizing inductance model is considered according to increasing magnetizing current. To determine the knee point of the *B-H* curve, the open-circuit test is carried out by connecting coil terminals of the MEH to the AC supply through an auto transformer (HANIL HT-3000) and power analyzer (YOKOGAWA WT1800). The knee point voltage can be measured through the measurement setup shown in Fig. 15.

The auto transformer is used to vary the voltage applied to the MEH at the power frequency. Since magnetic saturation will result in a dramatic decrease of L_m, the knee point of the saturation voltage can be estimated by measuring the changes of impedance of L_m and i_{Lm}. To confirm the knee point of the saturation, the applied voltage V_{app} from the auto transformer was increased from 15 V to 20 V in the experiment.

The values of L_m were measured and compared with those in the proposed saturable inductance model, as shown in Fig. 16. Values were nearly constant until the magnetic core became saturated. The value of L_m dramatically decreased when the applied voltage exceeded a certain point. As mentioned above, the knee point of the voltage is the point at which a 10 % increase in applied voltage increases i_{Lm} by 46.7 %. The knee point voltage in our design is found to be 15.2 V according to the power meter results shown in Fig. 17. Comparison with the measurement results was also conducted. In the proposed model, the saturable magnetizing inductance dramatically dropped near the knee point. The reason is that the proposed model reflects the knee point of the *B-H* curve near the saturation point. As a result, the proposed model is coincided more with the measured results in saturated conditions.

C. EXPERIMENTAL RESULTS FOR MAXIMUM HARVESTED POWER IN SATURATED CONDITION OVER WIDE PRIMARY CURRENT RANGE

The output model applying the proposed saturable magnetizing inductance model was verified through measurement. Fig. 18 shows the experimentally measured value of P_o and the numerically calculated P_o at adjusted V_{pri}. In linear operation, P_o is proportional to V_{pri}. The measured results and the

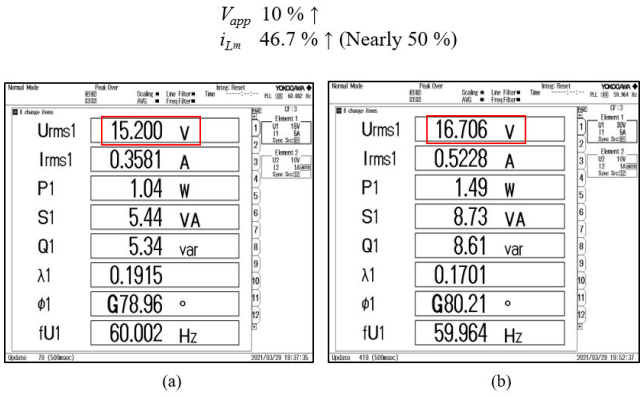

FIGURE 17. Accurate measurement results using power meter. (a) $i_{Lm} = 0.3513$ A, where $V_{app} = 15.2$ V; (b) $i_{Lm} = 0.515$ A, where $V_{app} = 16.7$ V.

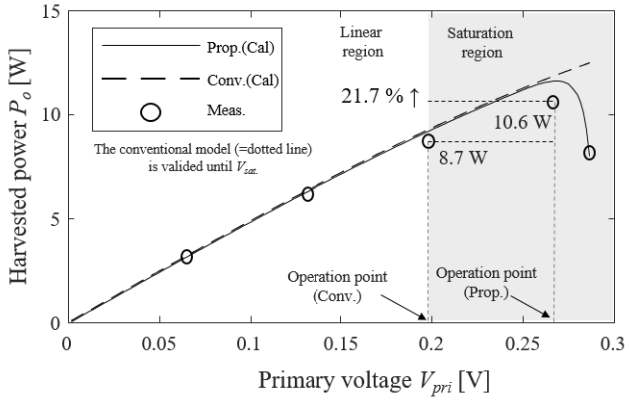

FIGURE 18. Numerical calculations and measurement results of harvested power P_o according to primary voltage V_{pri} by considering saturated conditions.

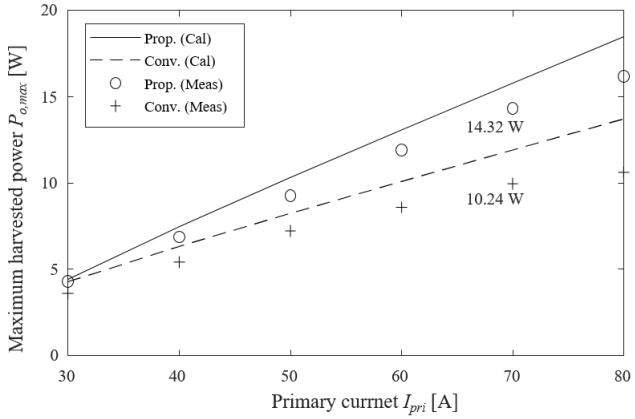

FIGURE 19. Maximum harvested power P_o according to primary side current I_{pri}.

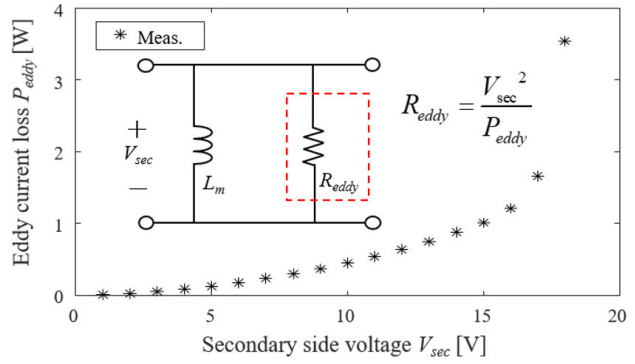

FIGURE 20. Measurement result of the open-circuit test for parameter estimation of eddy current loss.

numerical calculation matched well. The point of maximum harvested power is generated in the vicinity of the saturation point.

When the load voltage exceeds a critical saturation voltage, P_o dramatically decreases. The reason is that the value of L_m is reduced and, then, reactive power increases. The maximum harvested power has a value of 10.6 W at 55 A in the conventional design method. Compared with [29], we can achieve a value of 8.7 W near the saturation point, an increase of 21.7%, by applying the proposed design method. Moreover, the proposed model is found to agree better with the measurement results in saturated regions than does the previous model.

The output power of the proposed design methodology is analyzed according to different primary current. Fig. 19 shows the maximum harvested power according to the primary current. When the primary current is relatively low, the proposed design method shows a slightly higher harvested power than does the conventional model.

However, as the primary current range widens, the difference between the two design methodologies increases. Compared with [28], we can achieve a value of 14.32 W on 70 A, which is an increase of 39.8%, by applying the proposed design method. From this comparison, it can be seen that the proposed design method has an advantage of reducing core material.

IV. DISCUSSION

For simplicity of analysis, an effect of core loss for MEH can be ignored [17]. However, eddy current loss should be considered for accurate analysis of output model in conductive material [35].

Assuming that the core loss is equal to eddy current loss P_{eddy}, the effect of P_{eddy} on the magnetic core can be expressed with a resistance R_{eddy} in parallel with the L_m as shown in Fig. 20. To estimate circuit parameter, R_{eddy} is determined based on measurements by open-circuit test using a power meter. In our circuit analysis, the R_{eddy} is 250 ohm. Fig. 21(a) illustrates an example with $i_{pri,rms} = 55$ A, $N = 60$, and $V_{sec} = 9$ V respectively. In normal conditions, P_{eddy} of 0.26 W, which is 4% of output power is generated. As shown in Fig. 21(b), we also confirmed that P_{eddy} is increased according to V_{sec} and the ratio of P_{eddy} is increased.

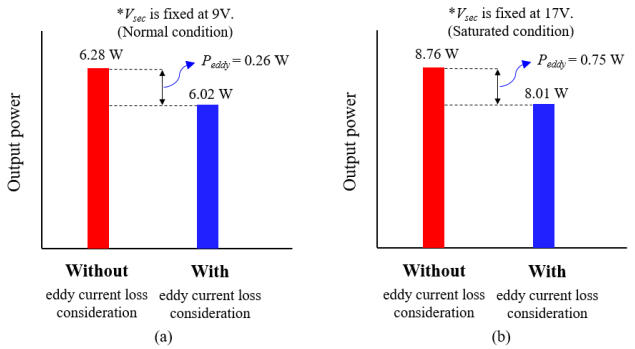

FIGURE 21. Circuit simulation results of including the eddy loss effect. (a) Normal condition(@V_{sec} = 9V). (b) Saturated condition(@V_{sec} = 7V).

For further research, the effect of loss including coreless and copper loss will be examined for accurate analysis and design.

V. CONCLUSION

In this paper, a practical design method of an MEH with improved power density was proposed for maintenance applications near power lines. The proposed method is different from the conventional design based on current transformer, which is focused on measurement in that it operates in the saturation condition. The main idea is to use the saturable magnetizing inductance model to determine the load voltage necessary to harvest maximum output. The design methodology for determining the load voltage has been explained by considering the nonlinear characteristic of the magnetic material. To consider the magnetizing current dependent inductance characteristics, the saturable magnetizing inductance model is used based on measurement data. This model is useful because it gives a guideline for the operation voltage range for maximum harvested power. To verify the proposed saturable magnetizing inductance model, experimental evaluation was conducted. To emulate a real power line, current source controlled through a 150 kW class AC resistor load bank is used. Based on the calculated and measured results, compared to conventional design methodology, the proposed design methodology was able to harvest 14.32 W on a 70 A_{rms} power line, which is an increase of 39.8 % compared with the conventional design method. In addition, the proposed design methodology can improve the power density and accurately estimate output power according to load voltage in saturated condition.

APPENDIX A

From Faraday's induction law, the induced voltage in the coil terminals can be determined as follows:

$$V = -N\frac{d\phi}{dt} \tag{20}$$

where N is coil winding turns and the ϕ is magnetic flux through a single loop.

When the magnetic core does not saturate until a maximum linear point, equation (20) can be derived through integrating on both sides over half-period.

$$\int_0^{\frac{T}{2}} V_{sat}dt = 2B_{\max}A_{eff}N \tag{21}$$

where T is primary side period and B_{max} is the saturation flux density. V_{sat} is saturation voltage and A_{eff} is the cross-sectional area of the magnetic core.

According to [17], the coefficient "2" before B_{max} on the left side comes from the phenomenon that the magnetic core goes from one end of the B-H curve($-B_{max}$) to the other end of the B-H curve($+B_{max}$) in a half period, which results in a total change of $2B_{max}$.

The V_{sat} can be expressed as follows:

$$V_{sat} \cdot \frac{T}{2} = 2B_{\max}A_{eff}N \tag{22}$$

$$V_{sat} = 4B_{\max}A_{eff}Nf \tag{23}$$

In this paper, all circuit components are reflected on the primary side($N = 1$) and then analyzed.

As a results, equation (23) can be rewritten as follows:

$$V_{sat} = 4B_{\max}A_{eff}f \tag{24}$$

APPENDIX B

The input current of sine-wave form can be determined as follows:

$$i(t) = A \cdot \sin(\omega_o t) \tag{25}$$

where A is amplitude of input current.

$$\phi(i) = \begin{cases} L_m i, & 0 \le \omega t \le \beta \\ L_m i_{sat}, & \beta \le \omega t \le \pi - \beta \\ L_m i, & \pi - \beta \le \omega t \le \pi \end{cases} \tag{26}$$

$$\beta = \sin^{-1}(i_{sat}/A) \tag{27}$$

where β is angular part, in which the magnetizing inductance maintains a linear value.

As mentioned Section II, the flux linkage verse the current curve can be substituted for the $L_m - i_{Lm}$ curve according to the definition of inductance.

Assuming the filtering hypothesis [30], the fundamental component must be considered, which can be described by

$$\lambda(t) \approx \lambda_1(t) = a_1\cos(\omega t) + b_1\cos(\omega t) = M\sin(\omega t + \theta) \tag{28}$$

where,

$$M(A,\omega) = \sqrt{a_1^2 + b_1^2} \text{ and } \theta(A,\omega) = \tan^{-1}(\frac{a_1}{b_1}) \tag{29}$$

To determine the coefficients of the fundamental frequency of Fourier series for the equation (28), the following equation can be described as follows:

$$a_1 = \frac{2}{\pi}\begin{bmatrix} \int_0^{\beta} L_m A\sin(\omega t)\cos(\omega t)d\omega t \\ + \int_{\beta}^{\pi-\beta} L_m i_{sat}\cos(\omega t)d\omega t \\ + \int_{\pi-\beta}^{\pi} L_m A\sin(\omega t)\cos(\omega t)d\omega t \end{bmatrix} \tag{30}$$

from which $a_1 = 0$,

$$b_1 = \frac{2}{\pi}\begin{bmatrix} \int_0^{\beta} L_m A \sin(\omega t)\sin(\omega t) d\omega t \\ + \int_{\beta}^{\pi-\beta} L_m i_{sat} \sin(\omega t) d\omega t \\ + \int_{\pi-\beta}^{\pi} L_m A \sin(\omega t)\sin(\omega t) d\omega t \end{bmatrix} \quad (31)$$

Form equation (30) and (31), the saturable magnetizing inductance $L_{m,sat}$ of equation (16) can be obtained. A more detailed description is described in [30].

ACKNOWLEDGMENT

The authors would like to thank the technical support from Ferraris Inc., and ANSYS Korea. (These contents are expected to be issued as a patent by 'Ferraris Inc.')

REFERENCES

[1] O. Menendez, F. A. Auat Cheein, M. Perez, and S. Kouro, "Robotics in power systems: Enabling a more reliable and safe grid," *IEEE Ind. Electron. Mag.*, vol. 11, no. 2, pp. 22–34, Jun. 2017, doi: 10.1109/MIE.2017.2686458.

[2] R. Moghe, F. C. Lambert, and D. Divan, "Smart 'stick-on' sensors for the smart grid," *IEEE Trans. Smart Grid*, vol. 3, no. 1, pp. 241–252, Mar. 2012, doi: 10.1109/TSG.2011.2166280.

[3] R. Moghe, A. R. Iyer, F. C. Lambert, and D. M. Divan, "A low-cost wireless voltage sensor for monitoring MV/HV utility assets," *IEEE Trans. Smart Grid*, vol. 5, no. 4, pp. 2002–2009, Jul. 2014, doi: 10.1109/TSG.2014.2304533.

[4] (Mar. 25, 2010). *Usi Power Donut Line Monitor*. [Online]. http://www.usi-power.com/power-donut-line-monitor/

[5] (Mar. 25, 2010). *Sentient MM3TM Intelligent Sensor*. [Online]. https://www.sentient-energy.com/products/mm3-intelligent-sensor/

[6] (Mar. 25, 2010). *LightHouse Medium Voltage Sensor*. [Online]. https://www.enghousenetworks.com/tollgrade/tollgrade-lighting-up-the-distribution-grid/

[7] (Mar. 25, 2010). *Franklin Electric Gridsense Line IQ*. [Online]. https://franklingrid.com/utility-grid

[8] S. Montambault and N. Pouliot, "The HQ LineROVer: Contributing to innovation in transmission line maintenance," in *Proc. IEEE 10th Int. Conf. Transmiss. Distrib. Construct., Operation Live-Line Maintenance, (ESMO*, Apr. 2003, pp. 33–41, doi: 10.1109/tdcllm.2003.1196466.

[9] S. Montambault and N. Pouliot, "LineScout technology: Development of an inspection robot capable of clearing obstacles while operating on a live line," in *Proc. IEEE 11th Int. Conf. Transmiss. Distrib. Construct., Operation Live-Line Maintenance (ESMO)*, Oct. 2006, pp. 1–9, doi: 10.1109/TDCLLM.2006.340744.

[10] I. Y. H. Gu, U. Sistiaga, S. M. Berlijn, and A. Fahlstrom, "Online detection of snowcoverage and swing angles of electrical insulators on power transmission lines using videos," in *Proc. 16th IEEE Int. Conf. Image Process. (ICIP)*, Nov. 2009, pp. 3249–3252, doi: 10.1109/ICIP.2009.5413984.

[11] Y.-p. Zhong, Q. Zuo, Y. Zhou, and C. Zhang, "A new image-based algorithm for icing detection and icing thickness estimation for transmission lines," in *Proc. IEEE Int. Conf. Multimedia Expo Workshops (ICMEW)*, Jul. 2013, pp. 1–6, doi: 10.1109/ICMEW.2013.6618443.

[12] J. Zhou, B. Zhang, W. Xiao, D. Qiu, and Y. Chen, "Nonlinear parity-time-symmetric model for constant efficiency wireless power transfer: Application to a drone-in-flight wireless charging platform," *IEEE Trans. Ind. Electron.*, vol. 66, no. 5, pp. 4097–4107, May 2019, doi: 10.1109/TIE.2018.2864515.

[13] M. Lu, M. Bagheri, A. P. James, and T. Phung, "Wireless charging techniques for UAVs: A review, reconceptualization, and extension," *IEEE Access*, vol. 6, pp. 29865–29884, 2018, doi: 10.1109/ACCESS.2018.2841376.

[14] S. Yuan, Y. Huang, J. Zhou, Q. Xu, C. Song, and P. Thompson, "Magnetic field energy harvesting under overhead power lines," *IEEE Trans. Power Electron.*, vol. 30, no. 11, pp. 6191–6202, Nov. 2015, doi: 10.1109/TPEL.2015.2436702.

[15] Z. Wang, J. Hu, J. Han, G. Zhao, J. He, and S. X. Wang, "A novel high-performance energy harvester based on nonlinear resonance for scavenging power-frequency magnetic energy," *IEEE Trans. Ind. Electron.*, vol. 64, no. 8, pp. 6556–6564, Aug. 2017, doi: 10.1109/TIE.2017.2682040.

[16] B. H. Choi, V. X. Thai, E. S. Lee, J. H. Kim, and C. T. Rim, "Dipole-coil-based wide-range inductive power transfer systems for wireless sensors," *IEEE Trans. Ind. Electron.*, vol. 63, no. 5, pp. 3158–3167, May 2016, doi: 10.1109/TIE.2016.2517061.

[17] J. Moon and S. B. Leeb, "Analysis model for magnetic energy harvesters," *IEEE Trans. Power Electron.*, vol. 30, no. 8, pp. 4302–4311, Aug. 2015, doi: 10.1109/TPEL.2014.2357448.

[18] N. M. Roscoe and M. D. Judd, "Harvesting energy from magnetic fields to power condition monitoring sensors," *IEEE Sensors J.*, vol. 13, no. 6, pp. 2263–2270, Jun. 2013, doi: 10.1109/JSEN.2013.2251625.

[19] W. Wang, X. Huang, L. Tan, J. Guo, and H. Liu, "Optimization design of an inductive energy harvesting device forwireless power supply system overhead high-voltage power lines," *Energies*, vol. 9, no. 4, pp. 1–16, 2016, doi: 10.3390/en9040242.

[20] B. Park, D. Kim, J. Park, K. Kim, J. Koo, H. Park, and S. Ahn, "Optimization design of toroidal core for magnetic energy harvesting near power line by considering saturation effect," *AIP Adv.*, vol. 8, no. 5, May 2018, Art. no. 056728, doi: 10.1063/1.5007772.

[21] P. M. Sánchez, F. J. R. Sánchez, and E. S. Gómez, "An experimental strategy for characterizing inductive electromagnetic energy harvesters," *Sensors*, vol. 20, no. 3, p. 647, Jan. 2020, doi: 10.3390/s20030647.

[22] P. Li, Y. Wen, Z. Zhang, and S. Pan, "A high-efficiency management circuit using multiwinding upconversion current transformer for power-line energy harvesting," *IEEE Trans. Ind. Electron.*, vol. 62, no. 10, pp. 6327–6335, Oct. 2015, doi: 10.1109/TIE.2015.2431648.

[23] Y. Zhuang, C. Xu, C. Song, A. Chen, W. Lee, Y. Huang, and J. Zhou, "Improving current transformer-based energy extraction from AC power lines by manipulating magnetic field," *IEEE Trans. Ind. Electron.*, vol. 67, no. 11, pp. 9471–9479, Nov. 2020, doi: 10.1109/TIE.2019.2952795.

[24] C. Song, H. Kim, Y. Kim, D. Kim, S. Jeong, Y. Cho, S. Lee, S. Ahn, and J. Kim, "EMI reduction methods in wireless power transfer system for drone electrical charger using tightly coupled three-phase resonant magnetic field," *IEEE Trans. Ind. Electron.*, vol. 65, no. 9, pp. 6839–6849, Sep. 2018, doi: 10.1109/TIE.2018.2793275.

[25] S. Paul, S. Bashir, and J. Chang, "Design of a novel electromagnetic energy harvester with dual core for deicing device of transmission lines," *IEEE Trans. Magn.*, vol. 55, no. 2, pp. 2019–2022, Nov. 2019, doi: 10.1109/TMAG.2018.2873012.

[26] Y. Liu, X. Xie, Y. Hu, Y. Qian, G. Sheng, X. Jiang, and Y. Liu, "A novel high-density power energy harvesting methodology for transmission line online monitoring devices," *Rev. Sci. Instrum.*, vol. 87, no. 7, Jul. 2016, Art. no. 075119, doi: 10.1063/1.4959556.

[27] R. H. Bhuiyan, R. A. Dougal, and M. Ali, "A miniature energy harvesting device for wireless sensors in electric power system," *IEEE Sensors J.*, vol. 10, no. 7, pp. 1249–1258, Jul. 2010, doi: 10.1109/JSEN.2010.2040173.

[28] L. Du, C. Wang, X. Li, L. Yang, Y. Mi, and C. Sun, "A novel power supply of online monitoring systems for power transmission lines," *IEEE Trans. Ind. Electron.*, vol. 57, no. 8, pp. 2889–2895, Aug. 2010, doi: 10.1109/TIE.2009.2037104.

[29] C.-Y. Lim, Y. Jeong, K.-W. Kim, F.-S. Kang, and G.-W. Moon, "A high-efficiency power supply from magnetic energy harvesters," in *Proc. Int. Power Electron. Conf. (IPEC-Niigata -ECCE Asia)*, May 2018, pp. 2376–2379, doi: 10.23919/IPEC.2018.8507990.

[30] S. C. Chung, E. C. Lee, S. R. Huang, and J. S. Huang, "Applications of describing functions to estimate the performance of nonlinear inductance," *IEE Proc. Sci., Meas. Technol.*, vol. 148, no. 3, pp. 108–114, May 2001, doi: 10.1049/ip-smt:20010368.

[31] A. Dayerizadeh and S. Lukic, "Saturable inductors for superior reflexive field containment in inductive power transfer systems," in *Proc. IEEE Appl. Power Electron. Conf. Expo. (APEC)*, Mar. 2018, pp. 3183–3188, doi: 10.1109/APEC.2018.8341557.

[32] C. Park, J. Park, Y. Shin, J. Kim, S. Huh, D. Kim, S. Park, and S. Ahn, "Separated circular capacitive coupler for reducing cross-coupling capacitance in drone wireless power transfer system," *IEEE Trans. Microw. Theory Techn.*, vol. 68, no. 9, pp. 3978–3985, Sep. 2020, doi: 10.1109/TMTT.2020.2989118.

[33] (Mar. 25, 2010). *Power Harvesting for Sensor in Electric Power Utility Applications: State of Science Review and Test Bed Development*. [Online]. https://www.epri.com/research/products/1024457

[34] (Mar. 25, 2010). *IEC 61869-2(Instrument Transformers—Additional Requirements for Current Transformers)*. [Online]. https://webstore.iec.ch/publication/6050

[35] J. Kim, K. Kim, H. Kim, D. Kim, J. Park, and S. Ahn, "An efficient modeling for underwater wireless power transfer using Z-parameters," *IEEE Trans. Electromagn. Compat.*, vol. 61, no. 6, pp. 2006–2014, Dec. 2019, doi: 10.1109/TEMC.2019.2952320.

BUMJIN PARK received the B.S. degree in electrical engineering from Chungnam National University, Daejeon, South Korea, in 2015, and the M.S. degree from The Cho Chun Shik Graduate School of Green Transportation, Korea Advanced Institute of Science and Technology, Daejeon, in 2017. He is currently pursuing the Ph.D. degree with the Korea Advanced Institute of Science and Technology. His research interests include simulation and development of energy harvesting systems.

SUNGRYUL HUH received the B.S. degree in electrical engineering from Incheon National University, Incheon, South Korea, in 2018, and the M.S. degree from The Cho Chun Shik Graduate School of Green Transportation, Korea Advanced Institute of Science and Technology (KAIST), Daejeon, South Korea, in 2020. He is currently pursuing the Ph.D. degree with KAIST. His research interest focuses on wireless power transfer system design for mobile device and electric vehicle.

JONGWOOK KIM received the M.S. degree from The Cho Chun Shik Graduate School of Green Transportation, Korea Advanced Institute of Science and Technology, Daejeon, South Korea, in 2017, where he is currently pursuing the Ph.D. degree. His current research interest includes the WPT.

HAERIM KIM received the M.S. degree from The Cho Chun Shik Graduate School of Green Transportation, Korea Advanced Institute of Science and Technology (KAIST), Daejeon, South Korea, in 2019, where she is currently pursuing the Ph.D. degree. Her current research interest includes the WPT.

YUJUN SHIN received the B.S. degree in electrical engineering from Inha University, Incheon, South Korea, in 2016, and the M.S. degree from the Cho Chun Shik Graduate School of Green Transportation, Korea Advanced Institute of Science and Technology, Daejeon, South Korea, in 2018. He is currently pursuing the Ph.D. degree with the Korea Advanced Institute of Science and Technology. His research interest focuses on wireless power transfer system design for electric vehicle and railway systems.

SEONGHO WOO received the B.S. degree in electrical engineering from Kyungpook National University, South Korea, in 2019, and the M.S. degree from The Cho Chun Shik Graduate School of Green Transportation, Korea Advanced Institute of Science and Technology (KAIST), Daejeon, South Korea, in 2021, where he is currently pursuing the Ph.D. degree. His research interests include electromagnetic interference and wireless power transfer.

JAEHYOUNG PARK received the M.S. and Ph.D. degrees from The Cho Chun Shik Graduate School of Green Transportation, Korea Advanced Institute of Science and Technology (KAIST), Daejeon, South Korea, in 2017 and 2020, respectively. He is currently a Staff Engineer with Samsung Electronics, Suwon, South Korea, where he is in charge of wireless charging system design.

ANDRES BRITO received the B.S. degree in electronics and control engineering from the Escuela Politécnica Nacional, Ecuador, in 2016, and the M.S. degree from The Cho Chun Shik Graduate School of Green Transportation, Korea Advanced Institute of Science and Technology (KAIST), South Korea, in 2020. He is currently pursuing the Ph.D. degree with KAIST. His research interests include wireless power transfer systems and SI/PI analysis in high-performance digital systems.

DONGWOOK KIM (Member, IEEE) received the B.Sc. degree in mechatronics engineering from Korea Polytech University, Siheung, South Korea, in 2014, and the M.Sc. and Ph.D. degrees in green transportation from the Korea Advanced Institute of Science and Technology (KAIST), Daejeon, South Korea, in 2016 and 2019, respectively. From 2019 to 2020, he was a Postdoctoral Researcher with the Department of Mechanical Engineering Research Institute, KAIST, and the Department of Mechanical and Manufacturing Engineering, University of Calgary, Calgary, AB, Canada. He is currently an Assistant Professor with the Department of Automotive Engineering, Yeungnam University, Gyeongsan, South Korea. His research interests include wireless power transfer system in microrobots, implantable devices, and electric vehicles.

HYUN HO PARK (Senior Member, IEEE) received the B.S. degree in electronic engineering from Pusan National University, Pusan, South Korea, in 1994, and the M.S. and Ph.D. degrees in electrical engineering from the Korea Advanced Institute of Science and Technology (KAIST), Daejeon, South Korea, in 1996 and 1999, respectively.

From 1999 to 2003, he was a Senior Research Staff Member with the Electronics and Telecommunications Research Institute (ETRI), Daejeon. From 2006 to 2012, he was a Principal Engineer with Samsung Electronics, Suwon, South Korea. He joined The University of Suwon, Hwaseong, South Korea, in September 2012, where he is currently an Associate Professor. His current research interests include computational electromagnetics, system-level electromagnetic interference (EMI) design, signal and power integrity in high-speed digital system design, and IC/module-level EMI evaluation and measurement techniques.

OKHYUN JEONG (Member, IEEE) received the B.S., M.S., and Ph.D. degrees in electronic engineering from Sogang University, Seoul, South Korea, in 1982, 1985, and 1996, respectively. From 1985 to 2012, he had worked as an Engineer, a Senior Executive VP, and the Head of the Mobile Communication Research and Development Center, LG Electronics, Seoul. Since March 2012, he has been an Associate Professor with the Department of Electronic Engineering, Sogang University. His research interest includes power consumption and thermal management model of mobile IoT device and wireless power charging system design for wearable robot.

JA-IL KOO received the M.S. and Ph.D. degrees from the Electrical Engineering Department, Korea Advanced Institute of Science and Technology, Daejeon, South Korea, in 1987 and 1991, respectively. From 1991 to 1993, he has worked as an Associate Professor with the University of Washington, Seattle, WA, USA. From 1994 to 1999, he has worked as a Staff Engineer with Siemens Medical System, Issaquah WA, where he was in charge of ultrasound Doppler system development. From 2000 to 2002, he has worked as a Staff Engineer with VLSI Technology, Pheonix, AZ, USA. He is currently the CEO of Ferraris Inc., Las Vegas, NV, USA, and has been developed magnetic harvesting device and system for last more than ten years. He has more than ten magnetic harvesting related international patents and published more than ten related articles.

SEUNGYOUNG AHN (Senior Member, IEEE) received the B.S., M.S., and Ph.D. degrees in electrical engineering from the Korea Advanced Institute of Science and Technology (KAIST), Daejeon, South Korea, in 1998, 2000, and 2005, respectively. From 2005 to 2009, he was a Senior Engineer with Samsung Electronics, Suwon, South Korea, where he was the incharge of high-speed board design for laptop computer systems. He is currently a Professor with The Cho Chun Shik Graduate School of Green Transportation, KAIST. His current research interests include wireless power transfer system design and electromagnetic compatibility design for electric vehicle and high-performance digital systems.